Front. Earth Sci. 2019, 13(1): 55–74
https://doi.org/10.1007/s11707-018-0707-y

RESEARCH ARTICLE

Quantitative analysis of planation surfaces of the upper Yangtze River in the Sichuan-Yunnan Region, Southwest China

Fenliang LIU[1], Hongshan GAO (✉)[1], Baotian PAN[1], Zongmeng LI[2], Huai SU[3]

1 Key Laboratory of Western China's Environmental Systems (Ministry of Education), College of Earth and Environmental Sciences, Lanzhou University, Lanzhou 730000, China
2 School of Geographic Sciences, Xinyang Normal University, Xinyang 464000, China
3 College of Tourism and Geography Science, Yunnan Normal University, Kunming 650500, China

Abstract Identification of the planation surfaces (PSs) is key for utilizing them as a reference in studying the long-term geomorphological evolution of the Upper Yangtze River Basin in the Sichuan-Yunnan region, Southwest China. Using a combined method of DEM-based fuzzy logic and topographic and river profiles analysis and based on a comprehensive analysis of four morphometric parameters: slope, curvature, terrain ruggedness index, and relative height, we established the relevant fuzzy membership functions, and then calculated the membership degree (MD) of the study area. Results show that patches with a MD > 80% and an area > 0.4 km^2 correspond well to the results of Google Earth and field investigation, representing the PS remnants. They consist of 1764 patches with an altitude, area, mean slope, and relief of mostly 2000–2500 m above sea level (asl), 0–10 km^2, 4°–9°, 0–500 m, respectively, covering 9.2% of the study area's landscape, dipping to southeast, decreasing progressively from northwest to southeast in altitude, and with no clear relation between each patch's altitude and slope, or relief. All these results indicate that they are remnants of once regionally continuous PSs which were deformed by both the lower crust flow and the faults in upper crust, and dissected by the network of Upper Yangtze River. Additionally, topographic and river profiles analysis show that three PSs (PS1–PS3) well developed along the main valleys in the Yongren-Huili region, indicating several phases of uplift then planation during the Late Cenozoic era. Based on the incision amount deduced from projection of relict river profiles on PSs, together with erosion rates, breakup times of the PS1, PS2, and PS3 were estimated to be 3.47 Ma, 2.19 Ma, and 1.45 Ma, respectively, indicating appearance of modern Upper Yangtze River valley started between the Pliocene to early Pleistocene.

Keywords planation surface, fuzzy logic, topographic analysis, river profile analysis, Upper Yangtze River, Southwest China

1 Introduction

Since the theory of the erosion cycle and the peneplain was put forward at the end of the 19th Century (Davis, 1889a, b, 1899), the planation surface (PS) has become one of the basic paradigms and theoretical parameters in geomorphology. Though the definition of PS has been widely discussed, PSs, such as peneplains, pediments, pediplains, and etchplains, generally are considered as land surfaces modelled by surface or near-surface wear on a rock mass, where the result of the wear is reasonably planar (planate) or slightly inclined. These nearly flat surfaces ranges from several km^2 to 10^5 km^2 (Guillocheau et al., 2018) and have to bevel the underlying basement structure and diverse bedrock types despite residual hills (Adams, 1975; Huggett, 2016). PSs have been widely recognized in many mountain belts worldwide (Calvet et al., 2015). As prominent and regional elements in present-day landscapes and excellent reference level indicators, PSs play an important role in the research of long-term landscape evolution (Bascom, 1921; King, 1962; Kennan et al., 1997; Widdowson, 1997; Japsen et al., 2009; Wang et al., 2012; Lidmar-Bergström et al., 2013; Coltorti et al., 2015). Over the past thirty years, stimulated by both the development of low temperature geochronological techniques (Bishop,

Received August 31, 2017; accepted February 9, 2018

E-mail: gaohsh@lzu.edu.cn

2007) and the advent of digital terrain analysis techniques (Pike, 2000), the field-work based study of PSs and other related features have been resurrected and greatly applied in the study of regional landscape, drainage basin and fluvial valley evolution, tectonic deformation, and mantle dynamics over geological timescales on every continent and in many mountain belts, for example in Africa (e.g., Coltorti et al., 2015; Guillocheau et al., 2018), the Pyrenees (e.g., Bosch et al., 2016), in Greenland (e.g., Bonow et al., 2006a, b, 2014), the Armorican Massif in the Western France (e.g., Bessin et al., 2015), in Scandinavia (e.g., Lidmar-Bergström et al., 2013), the Andes (e.g., Kennan et al, 1997), the Himalayas (e.g., van der Beek et al., 2009), the Tibetan Plateau (e.g., Hetzel et al., 2011; Li et al., 2018), and the Gobi Altai (e.g., Jolivet et al., 2007).

The Upper Yangtze River Basin (UYRB) in the Sichuan-Yunnan region (SYR), also known as the Jinsha River Basin, is located in the southwestern China, in the transition zone between the Tibetan Plateau and the Yunnan Plateau. The present-day topography of this region is highly unusual. It is characterized by a high altitude, low-relief plateau surface dissected by the deep valley system of the Yangtze River (Clark et al., 2006). A striking feature of all the mountain ranges in the region is the evenness of the summit levels. These upland low-relief surfaces have been studied by many researchers and most have agreed on the existence of one or more formerly planar and low, though now uplifted and deeply dissected, PSs (Huang, 1992; Wang et al., 1998; Feng et al., 2004; Zhou et al., 2005; Clark et al., 2006). Some scholars have also discussed the nature of these surfaces, e.g., Cui et al. (2001a) argued they are the double leveling surfaces of karst planation; Clark et al. (2006) thought that they are the remnants of a polygenetic surface formed at low altitude; Yang et al. (2015) argued that these surfaces were produced by river capture during drainage organization, instead of the remnants of a preexisted surface. However, an accurate description of these PSs is an essential prerequisite for PS analysis and to be useful as geomorphological markers.

In the past, PSs were usually mapped and delineated based on study of topographic maps combined with field investigation. This is a subjective and time-consuming analysis. Over recent decades, with the development of the Geographic Information System (GIS) and digital elevation models (DEMs), it has become possible for us to effectively recognize PSs over a regional scale. At present, a lot of works based on DEM-derived parameters with a hard threshold have been done to recognize the PSs (e.g., Ringrose and Migon, 1997; Johansson, 1999; Wang et al., 2005; Li et al., 2012; Rowberry, 2012; Veselský et al., 2015; Ma et al., 2016; Qian et al., 2016; Xiong et al., 2017). But PSs are ambiguous landforms; the boundaries between the PS and other landforms are usually not clear, especially when the original PSs were tectonically deformed or damaged by subsequent erosion. In such cases, obviously, the hard thresholds of the topographic parameters method are not suitable for describing such a fuzzy concept. Fuzzy logic methods (Zadeh, 1968), which are widely applied in geographic researches, have been introduced to PS research in recent years (Zhang and Huang, 1995; Haider et al., 2015). This method allows researchers to define the PS threshold class value by a smooth transition rather than by a hard threshold which better respects the character of the PS definition (Haider et al., 2015). In addition, topographic and longitudinal river profile analysis are other useful techniques for delineating the remnants of PSs or other relict landscapes, for where there are remnants of PSs dissected by valley networks, topographic and longitudinal river profiles on the relict landscape are characterized by significantly lower slope values than the surrounding incised landscape. Profiles across these regions are commonly interrupted by slope breaks or knickpoints (Schoenbohm et al., 2004; Rowberry et al., 2007; Legrain et al., 2014; Ma et al., 2016).

The aim of this paper is to identify and mapping the PSs of the UYRB in the SYR from the morphological perspective using a DEM-based fuzzy logic method combined with the topographic and longitudinal river profile analysis, and then to use the mapped surfaces as reference for a brief discussion of the long-term geomorphological evolution in this area.

2 Geological and geomorphological settings

In this paper, the UYRB in the SYR refers to the boundary area between the Sichuan and Yunnan provinces in southwestern China which is drained by the Upper Yangtze River system (Figs. 1(a) and 1(b)). Tectonically, this area is located between the Eastern Himalayan syntaxis to the west and the Sichuan Basin to the northeast and consists of two major crustal fragments. To the northwest is the Songpan-Ganze Block (SGB), to the southeast is the Yangzi Platform (YP) (Fig. 1(a)). Numerous faults are well developed bounding these blocks in this area, such as the Xiaojiang Fault (XJF), which is an active sinistral strike-slip fault, and the Yalong Thrust Fault Belt (YTFB), which consists of three to four parallel Cenozoic faults (Fig. 1(a); Wang et al., 1998). Since the Pliocene, this area has experienced drastic surface uplift as a result of upper-middle crustal shortening, lower crustal thickening, and the isostatic compensation due to surface erosion (Li et al., 2018).

From the geomorphological perspective, the large-scale landscapes of the UYRB in the SYR are characterized by a high altitude (1800–4500 m), low-relief (0–600 m) plateau with deeply incised valleys along the Upper Yangtze River and its main tributaries forming a local relief of ~2–3 km between mountain top and valley bottom (Royden et al., 1997; Clark et al., 2006; Liu-Zeng et al., 2008; Fig. 1).

From northwest to southeast, the mean altitude changes gradually from 4000–4500 m asl to 2000–2500 m asl but drops rapidly across the YTFB and the margins of the TP, forming topographical steps (Fig. 1(c); Liu-Zeng et al., 2008). Another marked characteristic of this area is that varied landforms, such as sharp or top-flat mountains, broad and shallow valleys, intermontane basins and lakes, and river gorges, are alternately distributed on the Plateau. Indeed, landscapes characterized by surfaces that appear in a series of steps are a common feature along the main river valleys in this area (Huang, 1992; Zhang et al., 1999). Especially in the Yongren-Huili region (Fig. 1), in fluvial valleys incised into the PSs, and along the main river valley, the landscape is commonly characterized by valley in valley or stepped surfaces; most rivers have not reached an equilibrium state (Yang et al., 2015).

3 Data and methods

3.1 DEM-based fuzzy logic analysis

Though the definition and formation mechanism of PSs are disputable, morphologically, the remnants of PSs all are

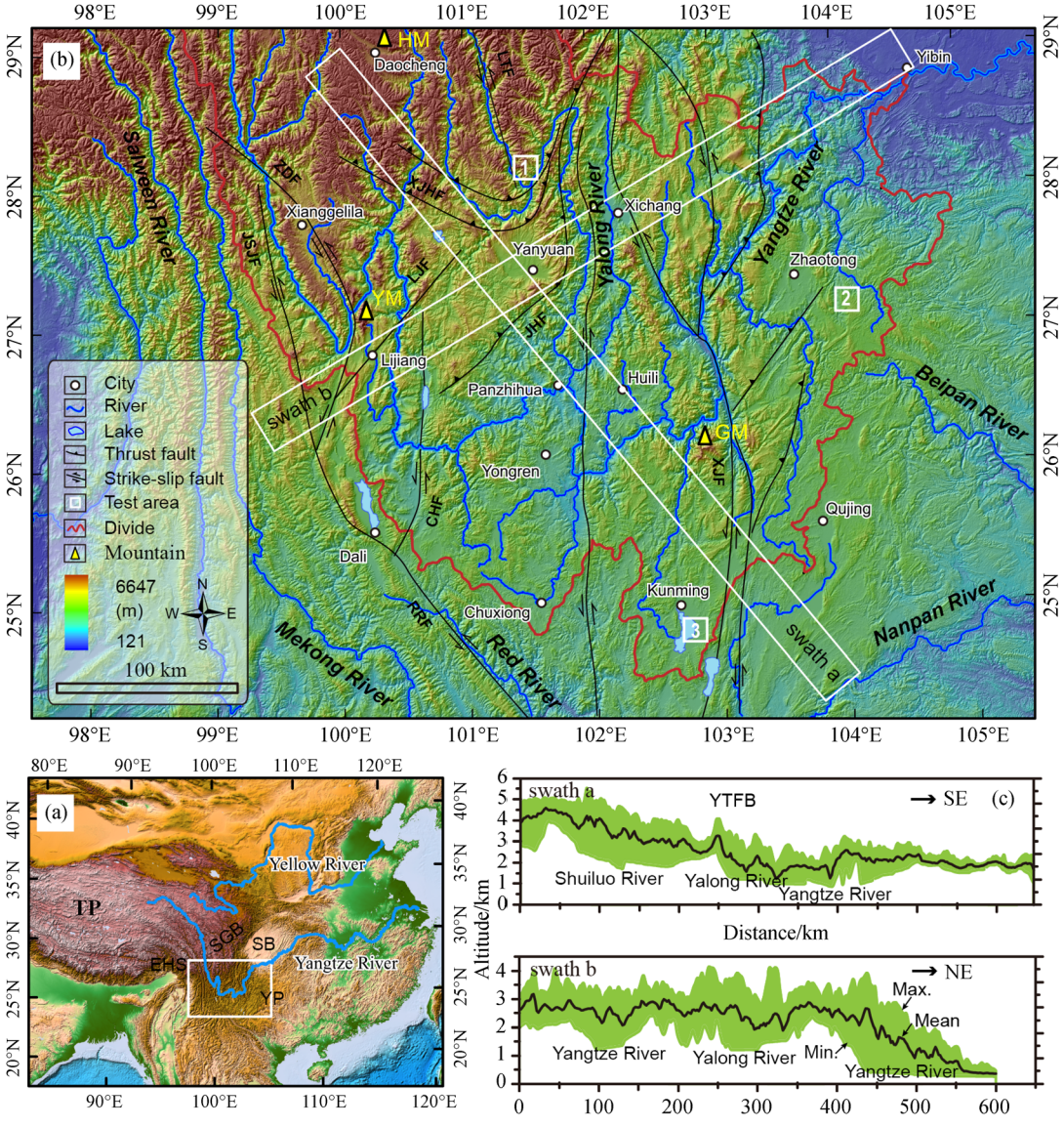

Fig. 1 The sketched map of the UYRB in the Sichuan-Yunnan region (SYR) and its surrounding regions. (a) Map showing location of the study area. (b) Topography with the main faults and rivers based on the shaded SRTM 90 m DEM. (c) Topographic profiles showing the mean, minimum, and maximum elevations in the 25 km swath: a and b in Fig. 1(b). XJF: Xiaojiang fault; ZMHF: Zemuhe fault; SMF: Shimian fault; LTF: Litang fault; XJHF: Xiaojinhe fault; JHF: Jinhe fault; LJF: Lijiang fault; CHF: Chenghai fault; LZJF: Luzhijiang fault; RRF: Red River fault; JSJF: Jinshajiang fault; ZDF: Zhongdian fault; TP: Tibetan Plateau; EHS: Eastern Himalaya Syntaxis; SB: Sichuan Basin; YP: Yangzi Platform; SGB: Songpan-Ganze Block; YM: Yulong Mountain; GM: Gongwang Mountain; HM: Haizi Mountain. YTFB: Yalong thrust fault belt.

characterized by sub-horizontal or slightly tilted top areas of mountains that form positive relief landforms elevated relative to the surrounding areas regardless of their genesis and age. These surfaces can be slightly undulating, but no well-developed valley system or intersecting river system exists on them. They are typically bordered by sharp morphological breaks, which separate the flat central landscape from the surrounding hilly lowlands. In addition, the flat-top character of these surfaces is not the consequence of sub-horizontal stratification of the substrate lithology or the sedimentary cover (Haider et al., 2013). So, the PSs can be characterized by a set of parameters describing the morphology of a flat-top mountain. In this study, we employed DEM-based fuzzy logic for multiple parameter assessment, following the method developed by Haider et al. (2015), to identify the PSs of the UYRB in the SYR. The principle of this method is that when a mountain landform with a flat top is relatively higher than its surroundings, this landform will have a great likelihood (membership degree) to belong to PS. In this method, a fuzzy logic procedure was used to convert the magnitude of the parameters to membership degree that a pixel under consideration belongs to a PS. Considering the manifestation of the PSs identified in this paper, the four morphological parameters, i.e., slope, curvature, terrain ruggedness index (TRI), and relative height (RH), which already used by Haider et al. (2015) were selected to describe the morphologies of the PSs of this area.

The SRTM v4 DEM was used for terrain analysis. This data has a horizontal resolution of 3 arc seconds (a ~90 m resolution) and a vertical error of < 16 m. The gap in areas of radar shadows was filled using a range of interpolation algorithms (Reuter et al., 2007; Jarvis et al., 2008). The requisite files were downloaded from the CGIAR-CSI GeoPortal. As PSs are large-scale geomorphic units (Kühni and Pfiffner, 2001; Guillocheau et al., 2018), the moderate DEM resolution is the most suitable, although terrain features are generalized and any smaller topographical details are inevitably lost. The higher resolution data contain much information that is of no use for the analysis of large landforms and may actually make the interpretation more difficult. So, considering our study area is very large, in order to speed the data process, the DEM data was resampled to a resolution of 250 m before analyzing. Previous studies have also demonstrated that DEMs at this scale provide useful tools for the identification of PSs (Bonow, 2004).

Slope is a maximum rate of change between each cell and its eight neighbor cells at the DEM (Burrough and McDonell, 1998). This parameter can detect the flat areas and excludes steep areas. But slope alone cannot detect potential PSs because other landforms, like lakes and alluvial basins, also are flat with low slopes. The slope is naturally limited to a value between 0°–90°. For the identification of PSs, the low slope data are relevant. However, PSs can be tilted by tectonic activity. Therefore, it is problematic to set an explicit boundary between 'still being a PS' and 'definitely not a PS'. With increasing slope, the likelihood of a possible PS decreases. Slope is calculated using the standard tools in a moving window of a 3×3 grid cell in ArcGIS.

Curvature for any direction is the second derivate of the surface or in other words, the slope of a slope (Zevenbergen and Thorne, 1987). It is broadly used in terrain analysis in hydrology and soil erosion studies (Zevenbergen and Thorne, 1987; Olaya, 2009; Peckham et al., 2011). Profile and plan curvature can be calculated. Negative values coincide with concave features. Positive values are related to the convex features. Zero value describes a flat surface independent of inclination. As a potential parameter for identification of PS, curvature distinguishes planar surfaces and excludes zones along mountain crests which cannot be distinguished by the parameter slope. Curvature with values near zero can characterize potential PSs. With increasing absolute value of curvature, the likelihood of a potential PS decreases. The curvature can be high only at the rim of the PS where the slope is sharply broken. Curvature is calculated using the standard ArcGIS module involving combined plan and profile curvature. The value of curvature range between -100 and $+100$ m^{-1}.

The TRI is the summed change in elevation between a grid cell and its eight neighbor grid cells (Riley et al., 1999). It was developed to characterize surface ruggedness and quantify topographic heterogeneity such as steep and dissected areas and undulating surfaces. The internal part of the PS, which has not been affected by rapid erosion, remains intact and flat, and is characterized by low TRI values. It is calculated by the following formula:

$$\mathrm{TRI} = \sqrt{x + 9v^2 - 2vs}, \tag{1}$$

where x is the focal sum of the squared DEM cells, v is the focal value, and s is the focal sum in the floating window 3 by 3 raster cells. The values of x, v, s are calculated using the neighborhood statistics and raster calculator tools in ArcGIS.

The RH, which is developed primarily to eliminate plain surfaces near local erosional base levels to delimit potential PSs, is an important parameter for the identification of PSs. It is defined as the vertical difference between the landscape surface and the envelope surface of the local base level represented by the main branches of the drainage system (Haider et al., 2015). The envelope surface was produced by an interpolation of the valley floors. So, the erosional base level is highly influenced by the considered drainage network. After a comparative analysis of the drainage systems with catchment areas > 10 km^2, > 50 km^2, > 100 km^2, and > 500 km^2, respectively, we found that the valleys with a catchment area threshold of 50 km^2 extended just a little below the flat-topped areas (PSs) (Figs. 2(a) and 2(b)). We therefore considered that their

valley floors were the most appropriate to be interpolated for use in our calculation of the envelope surface of the local base level. The RH was calculated based on the present-day landscape and this envelope surface derived from interpolation of the valley floors with a catchment area > 50 km^2 (Fig. 2(c)).

In order to set the fuzzy logic criteria for each parameter, we need to select several test areas to analyze the parameter characteristics of the PSs and other main geomorphic units in the study area. The strategies of test areas selection are that these areas must cover the main landform types of the study area. Besides PSs, sharp ridges and steep valleys, broad intermontane basins and valleys are also extensively distributed in the study area. After a careful investigation by using Google Earth, we finally selected three square sub-regions as the test areas for comparative analysis of the values of the parameters of these representative geomorphic units. They ranged from 'steep and dissected area', to 'PS region', to 'intermontane basin', respectively, and all contained 7921 pixels with an area of about 495 km^2 (Fig. 3(a)). These test areas represent most landforms of the study area. We found that the density scatterplots of the parameter values for different test areas were significantly different (Fig. 3(b)). The dataset of 'steep and dissected area' scatterplots covered nearly the whole graphic, while the datasets of 'PS regions' and 'intermontane basins' covered only a small part of each of the graphics. However, the 'PS region' and 'intermontane basin' could be clearly distinguished using scatterplots of curvature *versus* RH. In the 'PS region', the value of the slope was approximately between 0° and 30°, but mostly $< 10°$; the value of the curvature was approximately between -0.5 m^{-1} and 0.5 m^{-1}, but mostly between -0.2 and 0.2 m^{-1}; the value of the TRI was approximately 0–400 m, but mostly < 120 m; and the value of the RH was approximately 0–750 m, but mostly > 250 m (Fig. 3(b)). After a comprehensive consideration of these findings, we established four separate fuzzy trapezoidal membership functions for these four morphometric parameters (Fig. 4), which could discriminate the 'PS region' from other regions. The fuzzy logic criteria were set as follows:

For slopes between 0° and 10°, the value of the membership degree (MD) was set to 100%; between 10° and 30° this was changed linearly from 100% to 0%; $>$ 30° slopes were set to 0%. This membership function is same as that of Haider et al. (2015). For the curvature, > 1 m^{-1} or < -1 m^{-1} values were set to 0%; and -1– -0.2 m^{-1} and 0.2–1.0 m^{-1} values were changed linearly from 100% to 0%, respectively. For the TRI, values between 0 and 80 m were set to 100%; values between 120 m and 300 m were changed linearly from 100% to 0%; and values $>$ 300 m were set to 0%. For the RH, < 60 m values were set to 0%; > 250 m values were set to 100%; and > 60 m and < 250 m values were changed linearly from 0% to 100%.

Finally, according to the membership functions above (Fig. 4), we converted the magnitude of each parameter to its MD using the Fuzzy Logic Toolbox in MATLAB. Because each parameter cannot constrain the PS alone, in

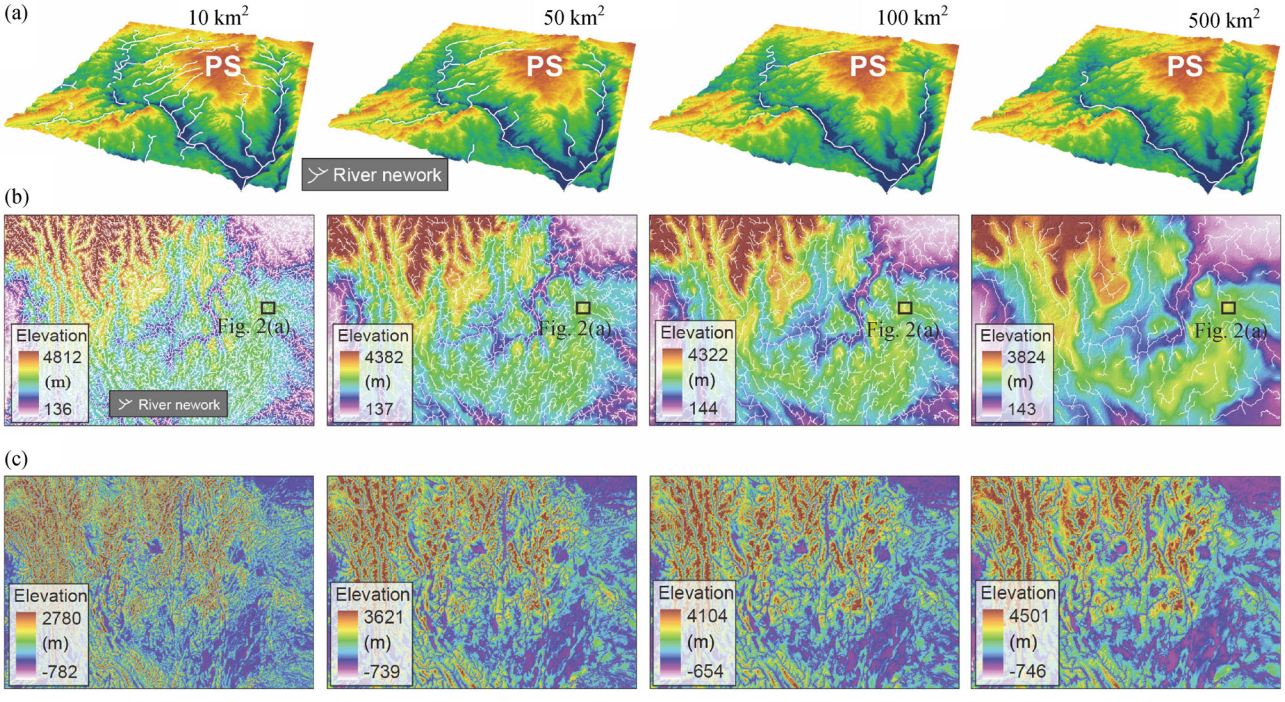

Fig. 2 Relative height based on different drainage area thresholds. (a) 3D DEM showing the typical planation surface (PS) with river of the black square region in Fig. 1(b); (b) Base levels with stream networks for interpolating; (c) Relative heights calculated from elevation differences between the base level and modern topography. PS: planation surface.

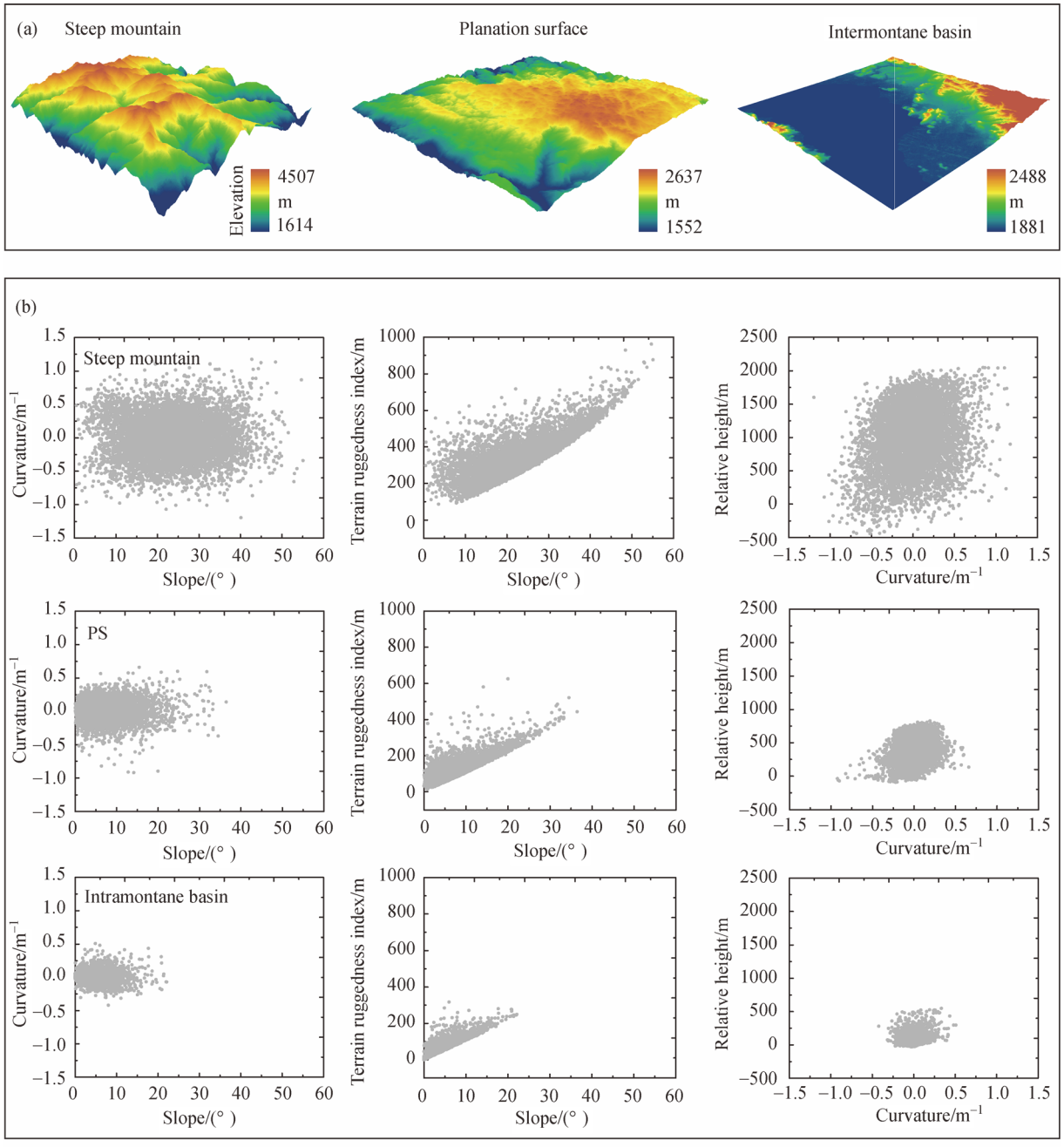

Fig. 3 Topographical characteristics of the test areas. (a) 3D view of the test areas based on SRTM 90 m DEM. (b) Density scatterplots of the morphometric parameters of the test areas.

order to get a joint assessment of the likelihood that a given area can be considered as a PS, we synthesized an integrative MD raster based on the MD raster for the four parameters above. The step was accomplished by using the raster calculator tool in ArcGIS. The value of each pixel of the integrative MD raster is the product of the corresponding pixels of the four MD raster, this means that a region will have a high integrative MD value only when the MD values for the four parameters in this region are all high. This integrative MD raster is shown in Fig. 5.

3.2 Topographic and river profiles analysis

In order to describe further the characteristics of the PSs and to analyze if the mapped remnants of the PSs represent one continuous surface or several PSs at different elevations, we analyzed the topographic and river profiles based on 90 m SRTM v4 DEM in the Yongren-Huili region where stepped surfaces are well preserved along the Upper Yangtze River valley.

Thirty-two (32) parallel individual topographic profiles

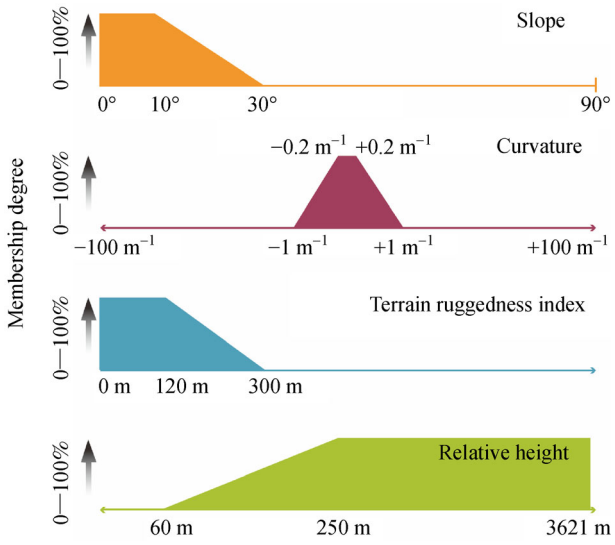

Fig. 4 Membership functions for the terrain parameters describing the PS remnants.

(Fig. 9(a)) were first constructed from DEM using Profile Graph tools in ArcGIS at regular intervals of 1.5 km. Data were exported to MS Excel and plotted in Origin. From these initial individual topographic profiles, a superimposed topographic profile was constructed. The result is shown in Fig. 9(d). Superimposed profiles were developed to allow the comparison and correlation of individual profile lines at regular intervals through the assimilation of each profile line into a single two-dimensional multiple line graph (Monkhouse and Wilkinson, 1952). Where there is a marked convergence in the superimposed profile graph of individual profile lines, a sub-horizontal PS may be indicated. If sub-horizontal surfaces are arranged in a stepped sequence, the convergence zone will be distributed at different altitudes.

Thirty-six (36) tributary channel profiles originated from the remnants of PSs along the Yangtze River in Yongren-Huili region (Fig. 9(a)) were selected to analyze by using the empirical relationship between drainage area A and slope S for an equilibrated channel (Hack, 1973; Flint, 1974):

$$S = k_s A^{-\theta}, \tag{2}$$

where θ and k_s are generally referred to as the concavity index and the channel steepness index, respectively (Wobus et al., 2006). River profiles, θ , and k_s were all extracted from 90 m SRTM DEM utilizing the stream profile tool for ArcGIS and MATLAB with procedures described in Wobus et al. (2006). Stream channels were sampled at a vertical interval of 20 m, then smoothed using a moving window of 1000 m. Because k_s is strongly related to θ, a normalized channel steepness index (k_{sn}) is often calculated using a fixed reference concavity index θ_{ref} = 0.45 which is the most commonly used value in the literature (Wobus et al., 2006). If the channel is considered to be in equilibrium (no knickpoints along the channel), only single values of θ and k_s should be fitted in a doubly logarithmic slope-area plot. If the channel is not in equilibrium, channel profiles will depart from the shape implied by the equations above. Thus, these relationships can also be used to identify different segments of the river profiles. The fit must then be done separately for the different segments of the channel. Here we use this latter approach as all channel profiles presented here have marked knickpoints. We also marked these knickpoints on each river profile.

4 Results and analysis

4.1 Test areas fuzzy logic method results and calibration of MD for the whole study

The spatial distribution of MD values (Fig. 5(a)) shows that the UYRB in the SYR has MD values ranging from 100% to 0%. Most of the study area has a very low MD, about half of the study area possesses a MD of $<$ 20%. These areas are mainly distributed in deep valleys, broad valleys, intermontane basins, and on sharp mountain crests, where, especially in the bottoms of valleys and basins, the MD is usually close to 0%, indicating that these landforms do not likely belong to the PS. The areas with a high MD occupy only a small part of the study area. For example, the areas with a MD of $>$ 80%, $>$ 90%, and 100% occupied 10.4%, 6.0%, and 0.6% of the total landscape of the study area, respectively. These areas are predominantly located on top or near-top areas of the topography, e.g., its river watersheds, interfluves between deep valleys, flat-top mountains above broad valleys or intermontane basins. Such areas have a high likelihood of

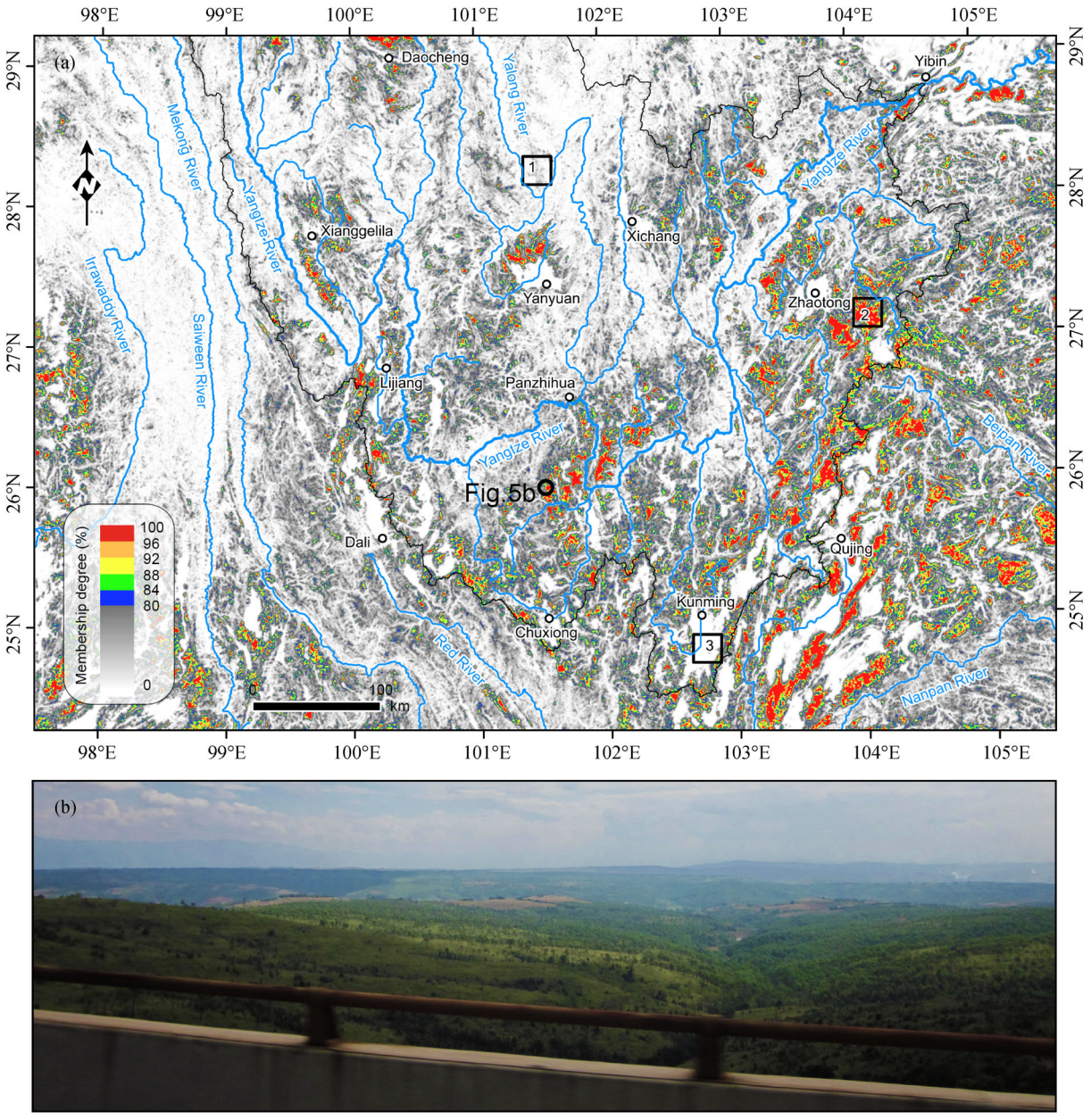

Fig. 5 The Membership degree (MD) and the PSs of the UYRB in the SYR. (a) Spatial distribution of the MD identified by the fuzzy logic integration of the four parameters. The squares with solid line edge indicate the locations of three test areas. (b) Field example of PS remnants. Photograph location is shown in Fig. 5(a).

belonging to the PS. Field investigation also showed that these areas with high MD values correspond to the low-relief, subdued regions (Fig. 5(b)). This would indicate that the MD map above can effectively identifies the potential remnants of PSs in the study areas.

The MD values in the three test areas are clearly different (Figs. 6(a) and 6(b)). The data for 'steep and dissected areas' have an MD of 0–76%, but the majority (85%) of this distribution lies between 0 and 20%. The data for 'intermontane basin' spreads over the whole MD scale but lies mostly (~82%) $<$ 50%. The MD data for 'PS region' range from 0% to 100%, but $>$ 92% have an MD of $>$ 80%. In order to select a suitable MD threshold to represent remnants of the PS in the study area, the results of interpretations from Google Earth images were compared to the results of various MD classifications in the test areas (Fig. 6(c)). In the steep mountain area with a MD of 0–76%, no PS was found based on the Google Earth images. In the intermontane basin area, a small PS patch was found from the Google Earth images where the MD is more than 80%. In the PS area, the PSs which we interpreted from the Google Earth images correspond well

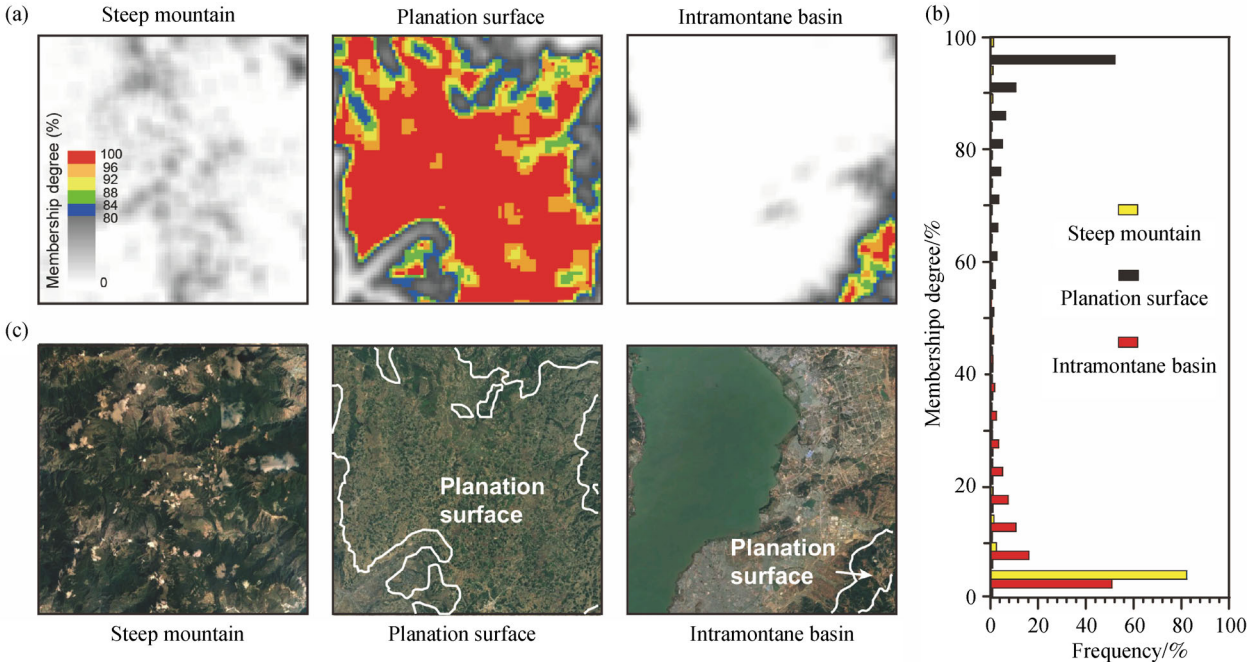

Fig. 6 Comparison between the MD and the Google Earth images in the three test areas. (a) The distribution of the MD. (b) Frequency histogram of the MD. (c) Google Earth images of the three test areas. The white polygons represent the remnants of PS which we interpreted from the Google Earth images.

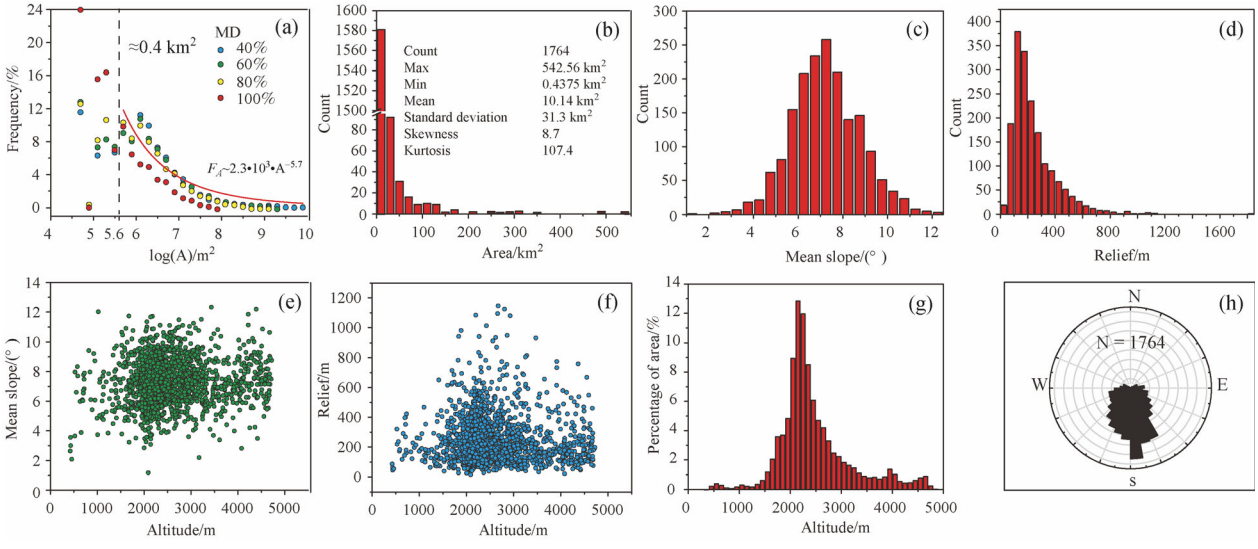

Fig. 7 Morphological characteristics of PSs of the UYRB in the SYR. (a) Frequency distribution of the area of the PSs of different membership degree thresholds. (b) Frequency distribution of the area of the PSs. (c) Frequency distribution of the mean slope of the PSs. (d) Frequency distribution of the relief of the PSs. (e) Relation between altitude and mean slope. (f) Relation between altitude and relief. (g) The altitude frequency distribution of the PSs. (h) Rose diagram showing the frequency distribution of the mean aspect of the PSs.

to the areas with a MD $>$ 80%. Therefore, a lower limiting MD of 80% was found to give the best correlation to the results of Google Earth interpretations. This value was then applied to all the studies areas (Fig. 5(a)). This value was also used by Haider et al. (2015) to represent the remnants of PS on the TP, the Andes, the Appalachian Mountains, the Northeast Iberia, the Massif Central, and the southern part of New Zealand (Haider et al., 2015).

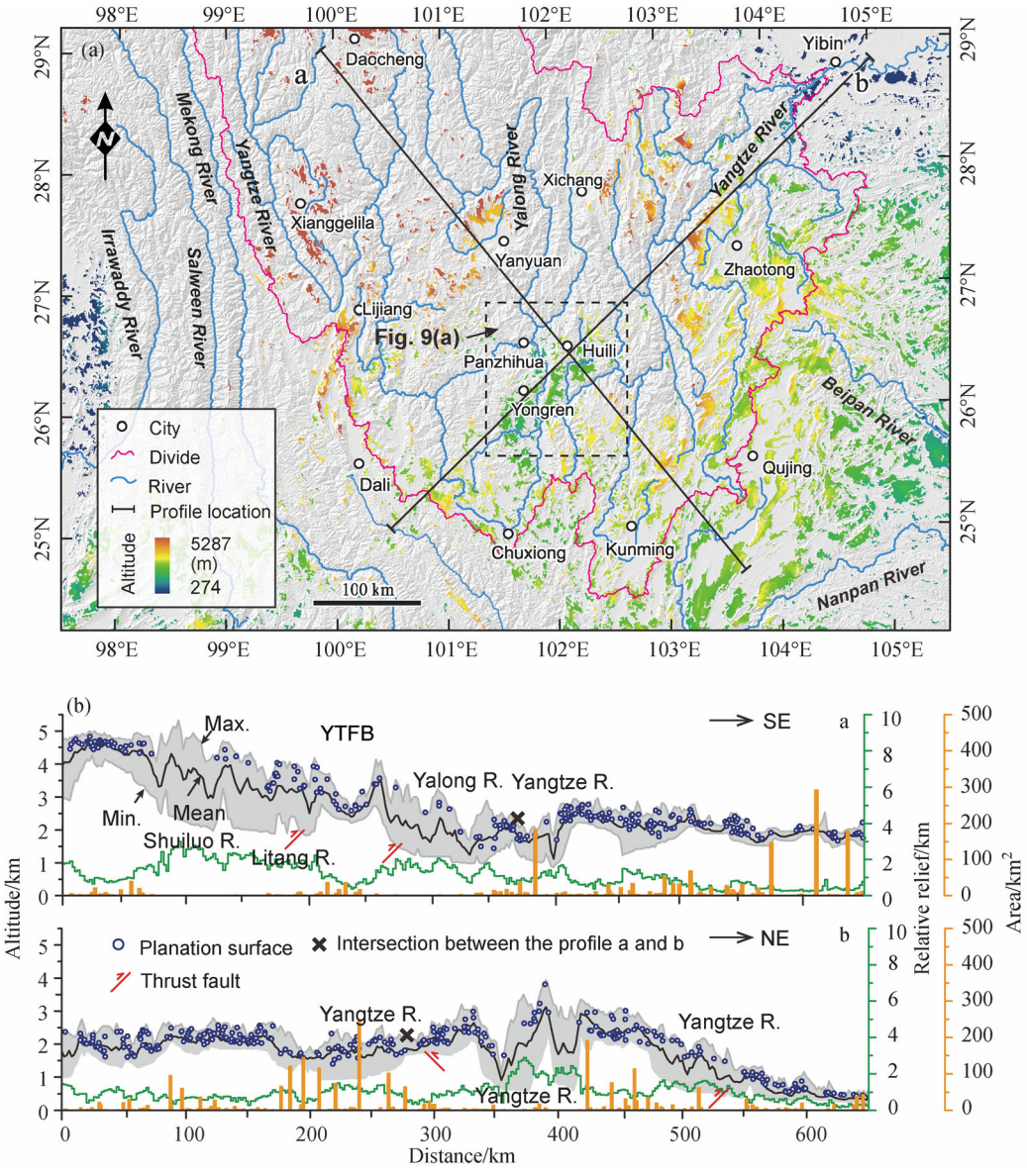

Fig. 8 PSs with a MD > 80% of the UYRB in the SYR mapped by this study. (a) Distribution of the remnants of PSs. The color represents its elevation. (b) The longitudinal relationship of topography (maximum, mean, minimum, and relief) and PS remnants elevations (mean) and areas within two 25 km wide swaths around two profiles a and b, respectively in Fig. 8(a).

4.2 Morphological characteristics and spatial distribution of PSs of the UYRB in the SYR

According to the above analysis, we extracted the PSs in the UYRB in the SYR using an MD threshold of 80% (Fig. 5). The PSs have a total number of 2585 isolated patches ranging from 0.0625 km^2 to 542.5 km^2 in area, giving a total area of 20,252 km^2. The frequency distribution of the area of the PSs was calculated and plotted in a semi-logarithmic plot (Fig. 7(a)), showing that the spatial extension of PSs has a complicated distribution with a marked cut-point at about Log (5.6) m^2, corresponding to ~0.4 km^2. When the patches are < 0.4 km^2, the relation between area and number is not clear. When the patches are > 0.4 km^2, the relation between area and number is negatively non-linear, and can be well fit using a power-law function, showing fractal characteristics. In addition, patches of an MD $> 60\%$, 70%, 90%, and 100% also analyzed for comparison; we found they all have such a property (Fig. 7(a)).

The common power-law relation between area and occurrence for patches > 0.4 km^2 is in agreement with the properties of a fragmentation process induced by a hydrographic network (Rigon et al., 1994). We therefore felt it reasonable to assume that the patches with an area $>$ 0.4 km^2 must be the remnants of PSs dissected by streams.

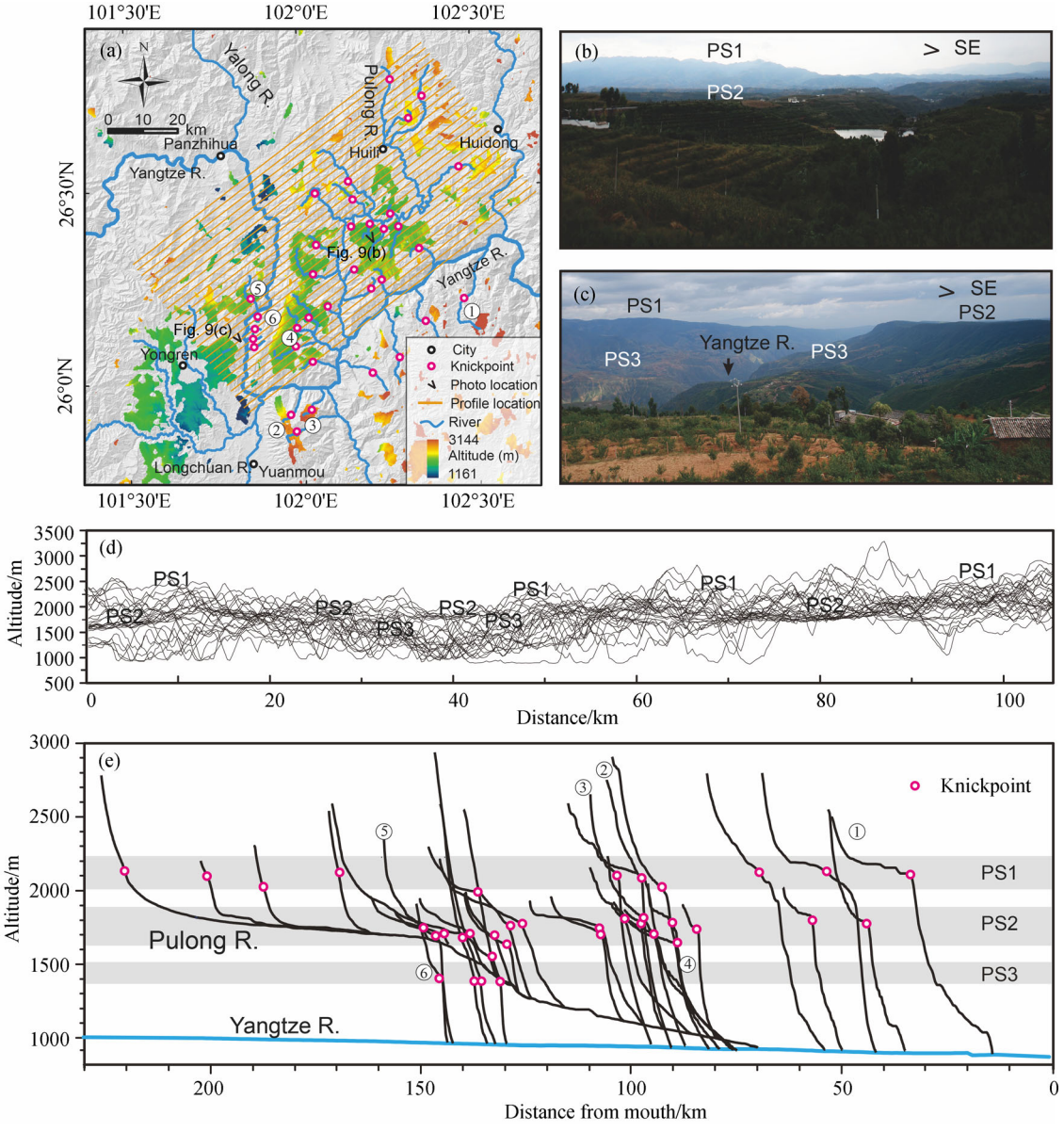

Fig. 9 PSs and topographical and longitudinal river profiles in the Yongren-Huili region. (a) Map of PSs with the main rivers in the Yongren-Huili region. (b) and (c) Field photographs of the PS. (d) Superimposed profile based on 32 individual topographic profiles in Fig. 9(a). (e) Longitudinal river profiles and knickpoints.

The unclear relation between area and number for the patches < 0.4 km^2 may have been complicated by the doping effect contributed by some other surfaces with no genetic relation to that PS, such as landslide benches, fluvial terraces, and artificial platforms (which may mathematically, but not geomorphologically, meet the criteria of a PS). Though the PS has no specified minimum or maximum areal dimension (Sevon et al., 1983), in order to exclude the influence of other original surfaces, we set 0.4 km^2 as a lower area threshold for PSs in this region, similar to that (0.5 km^2) set by Feng et al. (2004) in mapping PSs in the Dongchuan region, Yunnan Province.

After excluding the patches < 0.4 km^2 (851 patches with a total area of 2359 km^2), the PSs of the UYRB in the SYR total 1764 patches, ranging in area from 0.4375 km^2 to 542.5 km^2, with a significant standard deviation of 31.33 km^2, where the mean area is 10.14 km^2, the total area is 17,895 km^2 (Fig. 7(b)), and their total area covers ~9.2% of the total surface area of the study area. Small PSs are considerably more common than large PSs. 25.8% have an area of < 1 km^2. 82.5% of surfaces have an area of < 10 km^2. The mean slope of each PS ranges from 1.2° to 12.3°, with a standard deviation of 1.5°, mostly falling within the 4°–9° range (Fig. 7(c)); the mean slope of all PSs is 7.2°. The relief of individual PSs is between 15 m and 1820 m, with a standard deviation of 162.6 m. 52% of surfaces have

a relief of < 200 m, and 93% of surfaces have a relief of < 500 m (Fig. 7(d)). Scatterplots of slope *versus* altitude (Fig. 7(e)) and scatterplots of relief *versus* altitude (Fig. 7(f)) show that there is no clear relation between area and altitude, or between slope and altitude, for these patches. The distribution of mean aspects plotting in a rose diagram (Fig. 7(h)) shows that, though these patches evince a wide range in dip values, a preferential aspect between ~125° and ~180° can be found, indicating that these patches overall dip toward the southeast.

The spatial distribution map of these patches (Fig. 8) shows that the PSs of the UYRB in the SYR are widely distributed at altitudes ranging from 4851 m to 386 m asl. But the distribution is discontinuous and scattered, and is spatially and altimetrically uneven. The PSs located mostly at an altitude of 2000–2500 m asl (Fig. 7(g)). The most and largest surfaces are preserved in the south of the YTFB, especially in the watershed areas between the UYRB and the Red River, Nanpan River, and Beipan River basins to the south. PSs are relatively fewer and smaller in the YTFB and the northern sector of the YTFB, especially along the major tributaries of the Yalong, Anning, Shuiluo, and Shuoqu rivers where they are characterized by dense drainage networks and a dense alternation of V-shaped valleys and sharp crests, with narrow interfluves between the main river valleys. A strong link exists between the preservation of PSs and local relief (Fig. 8(b)). In areas with high local relief, patches of PS are few and are of small area. In areas with low local relief, patches are greater in number and area, this indicates that the spatial distribution of PSs reflects the erosional conditions prevalent in the study area, which depend on various factors such as structural conditions, positive diastrophism, the localization of river erosion, and various feedback mechanisms (Twidale, 1976). Therefore, the lack of PS remnants does not necessarily mean that they never formed. In fact, they could have been eroded away through the down-wearing of interfluvial areas after the active intersection of valleys.

Overall, from northwest to southeast, the mean altitude of these patches progressively decreases, from southwest to northeast, the mean altitude of the whole area increases slowly, but then drops acutely down toward the Sichuan Basin. On a small scale of tens of kilometers, the mean altitude of these remnants of PSs can vary up to several hundred meters, and often exhibits a rapid change across major known thrust faults, especially thrust faults like the YTFB (Fig. 8(b)).

4.3 Topographic and river profiles along the main river in the Yongren-Huili region

On the superimposed topographic profile derived from 32 individual topographical profiles (Fig. 9(d)), several distinct regions of marked topographic accordance can be clearly recognized. Overall, these sub-horizontal regions are distributed at three different altitudes along main river valleys. The highest surface is widely distributed between 2000–2400 m asl and is composed principally of the flat tops of mountains. This surface have been seriously dissected by rivers. The median surface developed well below the highest one, with an altitude of ~1600–1800 m asl. This surface is well-preserved around the highest one and is mainly represented by the middle shoulders along the main river valley, and dips slightly to the river valley. The lowest surface is limitedly distributed along the main river from Panzhihua to Yuanmou and an altitude from 1400–1500 m asl. This surface is represented by the lower shoulders of the v-shaped modern river valley.

Longitudinal river profile analysis (Figs. 9(e) and 10) showed that all tributaries are characterized by downstream portions with high k_{sn} values (e.g., > 286.11 for $\theta_{\text{ref}} = 0.45$) and irregular curves that are separated by one or more slope-break knickpoints from upper sections with low k_{sn} values and smooth curves (e.g., < 41.63 for $\theta_{\text{ref}} = 0.45$) (Fig. 11), suggesting the existing of relict surfaces. When we put these river profiles and knickpoints in the same coordinate (Fig. 9(e)), we found that these knickpoints are generally grouped at three distinctly altitudes, corresponding well to the altitudes of the three sub-horizontal surface levels identified by topographical profiles analysis.

5 Discussion

5.1 Origin of the upland low-relief bedrock surfaces in the UYRB

High altitude, low-relief surfaces are widely distributed on the mountain tops in the southeastern TP (Clark et al., 2006), but the origin of these surfaces has been disputed. Two major alternative mechanisms were proposed: dissection of a preexisting, low-relief landscape (Clark et al., 2006; Cui et al., 2001a) versus *in situ* formation of low-relief landscape patches in response to a rise in local base level following drainage area loss (Yang et al., 2015).

The upland low-relief surfaces produced by the two mechanisms above can be easily distinguished morphologically. According to the diagnostic criteria developed by Whipple et al. (2017), the essential, diagnostic characteristics of the upland low-relief surfaces formed by dissection of a preexisting, low-relief landscape is that the remnants of the surface are all preserved at a common elevation (allowing for variability in the relief and regional dip of the initial low-relief landscape) at all times; the low-relief headwater areas ultimately preserved as low-relief surface remnants are always the high points in the landscape. In addition, knickpoints that demarcate the boundary between upstream, relict channel reaches with low steepness and downstream, adjusted channel reaches with high steepness are predicted to occur at approximately equal elevations in channel profiles throughout the land-

scape (Niemann et al., 2001; Wobus et al., 2006). By contrast, surfaces produced by drainage capture mechanisms are predicted to be distributed randomly in elevation, to vary significantly in relief, to be bounded by drainage divides defined by the affected tributaries, and to be surrounded by a rim of high relief topography that persists until the final stages of landscape response to drainage reorganization. In addition, because relief reduction occurs during surface uplift, surface elevation and the degree of relief reduction will be strongly correlated.

When compared with the high altitude, low relief surfaces mapped by Clark et al. (2006) based on a slope between 1.2°–10° and a relief of <600 m in the southeastern of TP (Fig. 10(a)), including the bedrock surfaces and sedimentary basin surfaces, the surfaces mapped by this study are essentially distributed within the

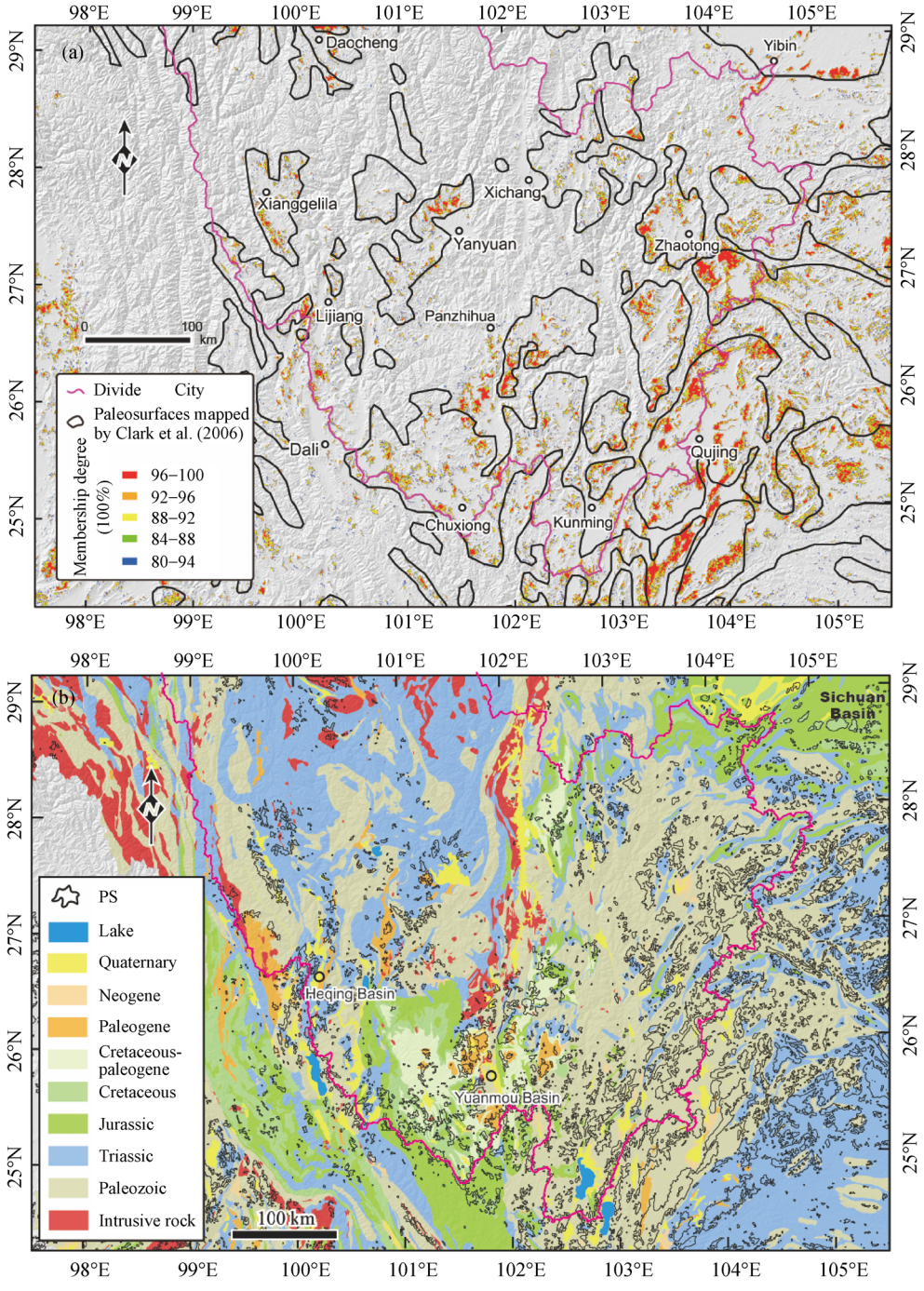

Fig. 10 PS remnants represented by the MD $>$ 80% in this study. (a) Relation between the PS remnants mapped by this study and the paleo surfaces mapped by Clark et al. (2006). (b) Relation between the PSs remnants mapped by this study and the simplified geological map based on the 1:2,500,000 Chinese geologic maps (Ministry of Geology and Mineral Resources).

ambit of the surfaces mapped by Clark et al. (2006), but are more intensely fragmented and spatially discrete. They are mostly distributed on the interfluves and river source areas and mountain tops between intermontane valley basins. They constitute only a small fraction (~24.6%) of the high altitude, low relief plateau surfaces which include all erosional and depositional flat areas just above the deeply dissected valleys. When comparing these surfaces with the regional geologic maps (Fig. 10(b)), we found that most of them cut across the bedrock of various complex compositions, resistances, and ages, therefore the surfaces we mapped in this study are all bedrock surfaces generated by erosion. Although these surfaces have been intensely deformed by faults and modified by streams, they are approximately co-planar and decrease in altitude systematically from northwest to southeast across the study area. Moreover, there is no relationship between the surface elevation and surface relief or surface slope (Figs. 7(e) and 7(f)). In addition, knickpoints on river profiles bounding the surface patches are grouped at altitudinal zones within which the corresponding PSs lie (Fig. 9(e)). According to these characteristics, it is clear that these surfaces are not compatible with those produced by the river piracy model. Therefore, the most likely interpretation for these upland low-relief surfaces of the UYRB in the SYR are that they are remnants of preexisting PSs that formed at low elevation, and were subsequently uplifted and dissected by the river systems.

5.2 Number and age of PSs and correlation

The question about the number and age of PSs that developed and survived in the UYRB is disputed (Huang, 1992). It is also difficult to elucidate how many PSs existed in this region because of the discontinuous nature of the preserved remnants, the tectonic deformation, and the lack of detailed information. As a working hypothesis, it is proposed that the leveled summits of the ranges along with the fluvial divides in a geological unit are remnants of a single major PS formed mainly by fluvial systems eroding to a common base level (Ahnert, 1998; Zárate and Folguera, 2014). The remnants of PSs we mapped in this study were distributed on the mountain top or fluvial divides at every major geological unit: the YP, the SGB, and the YTFB in the UYRB (Fig. 5 and Fig. 7). Though remnants in different tectonic blocks have different elevations, overall, the elevation change between these blocks is continuous and systematic, even across major faults (Fig. 7(b)). Therefore, we argue that these mountain-top surfaces are all the remnants of a once single regional PS, which formed at a common base level, but now is uplifted differentially and dissected unevenly. These surfaces are the major PS in this region, and are named PS1. According to the topographical and river profile analysis combined with field investigation in the Yongren-Huili region, below the PS1 there are another two lower sub-horizontal surfaces (labeled as PS2 and PS3, respectively) well developed along the main river valleys (Fig. 9). They take the form of wide valleys, and are not related to the faults. PS2 and PS3 have also been identified by other researchers around Yuanmou basin (Zhang et al., 1999). So, we suggest that at least three levels of PSs were developed and preserved in the UYRB.

Assuming that once the PS was uplifted, any river draining across it will immediately incise down in response to the change in base level, the age of this PS can be established by calculating the amount of time (Δt) required by the river to incise its valley to the modern-day location. The Δt was calculated using the method as follow (Kirby et al., 2010; Kirby and Whipple, 2012):

$$\Delta t = \Delta z/(E_c - E_h), \tag{3}$$

where E_c and E_h are the erosion rates within the river valley and on the PSs, respectively; Δz is the amount of incision into PSs. The Δz was estimated by projecting "relict" river segments based on steepness and concavity indices above knickpoints, assuming that they had concave profiles in equilibrium with prevailing conditions prior to the onset of base level fall (Schoenbohm et al., 2004; Clark et al., 2005; Harkins et al., 2007; Miller et al., 2013; Legrain et al., 2014). Δz is equal to the difference between the projected and modern channel elevations.

Although there are many tributaries along the Upper Yangtze River, and most of them featured transient behavior, the relict segments of most rivers have incised deeply and do not flow directly on PSs, other rivers that flow directly from PSs usually have too small of a relict segment to be reliably projected downstream due to the fact that PSs were seriously fragmented (Fig. 9). So, only a few tributaries were found to be suitable for reconstruction. The Yongren-Huili region, where remnants of PSs were well preserved, is the best region to calculate the Δz from each PS. In this region, we can only select six tributary rivers, where the channel profiles above the knickpoints were nearly in equilibrium; three rivers originate from the PS1, two rivers from the PS2, and one from the PS3 (Figs. 9 and 11). Following the method and procedures developed by Foster and Kelsey (2012) and fixing θ equal to 0.45, we project the relict channels above the major knickpoints to the confluence of modern river valley (Fig. 11). Through subtracting the modern outlet elevation of each tributary, Δz for these six rivers from PS1, PS2, and PS3 in the Yongren-Huili region have been calculated to be 1179±7.3 m, 1023±7.3 m, 925±6 m, and 690±10 m, 671±1 m, and 431±5 m, respectively (Fig. 11).

Previous research based on thermochronometry has shown that the long-term (from ca. 100 to ca. 20 or 10 Ma for PSs, and from ca.13 or ca. 9 Ma to present for river valley) erosion rates of the PSs and deep river valley in this region are ~0.02 mm/yr and ~0.25–0.5 mm/yr, respectively

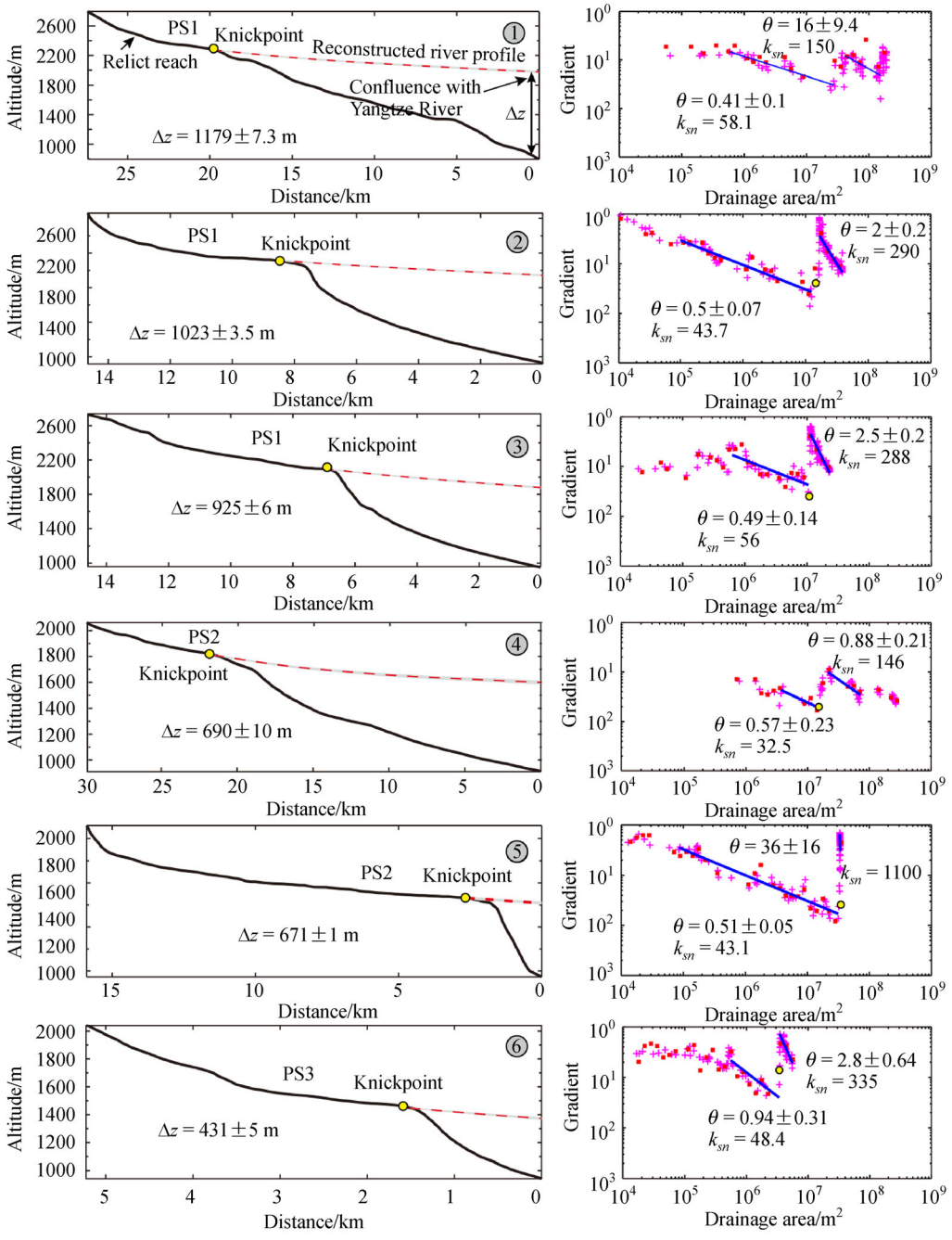

Fig. 11 Modern and reconstructed channel profiles for tributaries along the Upper Yangtze River. The 2σ elevation errors are from the normalized steepness indices and are based on linear regressions through log-log channel slope-drainage area data. For location of the channels refer to Figs. 9(a) and 9(e).

(Clark et al., 2005). According to Eq. (3), Δt for the PS1, PS2, and PS3 was calculated to be 5.16–1.91 Ma BP, 3.04–1.40 Ma BP, and 1.90–0.89 Ma BP, respectively. This would render a mean formation time of 3.47 Ma BP, 2.19 Ma BP, and 1.45 Ma BP, for these PSs, respectively. There is also other evidence to support this argument. The PS1 are locally unconformably overlain by flat-lying coal-bearing Pliocene sediments (Wang et al., 1998), suggesting this surface formed prior to the Pliocene. The basal ages of the sediment based on the palaeomagnetic analysis in the Yuanmou Basin (Zhu et al., 2008) and the Heqing Basin (Shen et al., 2010) in the study area which indicated the uplifting and disintegrating time of the PS1, dated to 4.9 Ma and 2.8 Ma, respectively. The sedimentation rate of the Yinggehai-Song Hong Basin in the South China Sea was relative low in the Middle Miocene–Early Pliocene, indicating a low relief landscape corresponding to PS1. The sedimentation rate became sharply higher since the

Early Pliocene (5.5 Ma, Clift and Sun, 2006; Lei et al., 2015), indicating a high relief landscape following the breakup of PS1. The erosion surfaces in the Dongchuan areas which correspond to PS2 or PS3 dated to 1.87 Ma based on the overlying fluvial deposits by ESR (Su et al., 2013).

PSs have been widely reported by many researchers on the TP and its surrounding mountains (Shackleton and Chang, 1988; Li et al., 1995; Cui et al., 2001a; Strobl et al., 2010). According to the age of PSs, the PS1 which is the major surface of the UYRB in the SYR could be correlated regionally with other well-known PSs. The Main Surface (4500–5000 m asl) on the TP with an age of 3.4–3.8 Ma obtained by dating the overlying basalt of the Mangkang Mountain in the southeast margin of TP using K-Ar dating method (Li, 1999; Fig. 12) and the E'xi Surface (1200–1500 m asl) at the Yangtze Gorges area (Xie, 1990) which probably formed at 3.4–3.6 Ma (Li et al., 2001, Fig. 11) correlate well in time with PS1. In addition, weathering materials of these PSs also have very similar or consistent properties which only developed under a hot and humid environment (Cui et al., 2001b). Taken together, these data indicate that these PSs may be the remnants of a single PS formed by eroding to a common base level, probably the sea level during their formation period.

5.3 Implications for regional deformation and long-term geomorphological evolution in the UYRB

PSs are important geomorphological markers for studying the regional land surface deformation and geomorphological evolution over a large spatial and temporal scale (Bessin et al., 2015; Coltorti et al., 2015; Li et al., 2018), and are often considered as the starting point for the modern drainage and valley system evolution (Pan et al., 2012; Vandenberghe, 2016).

If the Main Surface, PS1, and E'xi surface of the TP, the Yunnan Plateau, and the Yangtze Gorges region respectively are the remnants of a single PS, these original surfaces should be slightly undulate and have similar altitudes close to a distinct base level (possibly sea level) to which the rivers graded. At present, the PS remnants of different geological units in southeastern TP are all at high altitude; the altitude of these remnants varies regionally, deceasing from 5000 m asl on the TP to 2000 m on the Yunnan Plateau to 1000 m asl at the Yangtze Gorge region, showing a long-wavelength surface deformation (Fig. 12). This indicates that the land surface of the southeastern TP may have been subjected to an intense and differential surface uplift since the Pliocene (Li et al., 2018). The surface uplift of this region on such a large scale was most likely due to the crustal thickening from the eastward flow of the lower crust from the TP (Royden et al., 1997; Clark and Royden, 2000). The altitude of these remnants changes sharply across the major faults by several hundred of meters on small scale distances of tens of kilometers (Fig. 8 (b)), indicating that the PSs have also been seriously affected by local active faults. This implies that the upper crustal shortening cannot be ignored for crustal shortening in some local areas of the southeastern TP as suggested by Li et al. (2018).

Long-term geomorphological evolution of the UYRB in SYR since the Pliocene was roughly established (Fig. 13). PS1 was formed in the Middle Miocene to the Early Pliocene. During this period, the landscape of the UYRB appears to have had a subdued relief and may have slightly dipped to the southeast. The drainage networks in this period may have flowed to the South China Sea through the paleo Red River (Clark et al., 2004; Zheng et al., 2013), but they are likely to bear no correlation with the modern network of the Upper Yangtze River. PS1 began to uplift and disintegrate due to the intense tectonic movement in the Early Pliocene (Wang and Burchfiel, 2000; Li et al., 2018), possibly 3.4–3.6 Ma (Li, 1999). This tectonic movement is also known as the Hengduan Movement in the southeastern TP (Chen, 1992). In this period, basins on the plateau started to form and to receive deposits. Drainage networks on PS1 rejuvenated and began to incise. When rivers reached equilibrium again, PS2 developed by river lateral planation along the major valleys during the Early Pleistocene. Afterward, PS2 was uplifted at about 2.2 Ma, and PS3 developed locally. Following an accelerated tectonic uplift at about 1.5 Ma, the channel gradient increased and the Upper Yangtze

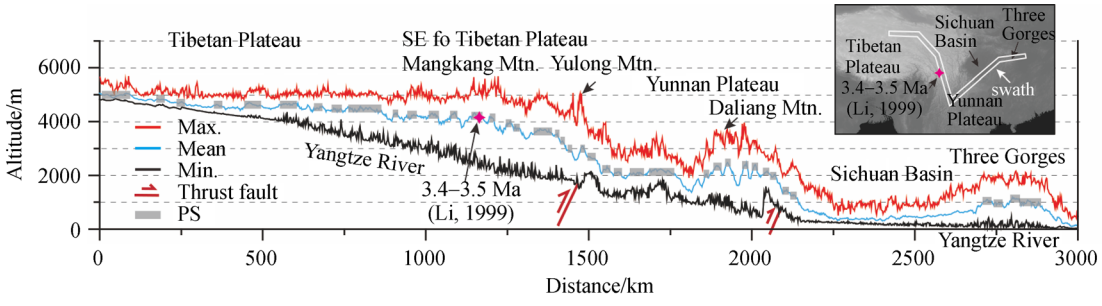

Fig. 12 Maximum, mean, and minimum topography along a 100 km wide swath window showing the spatial topographical change of the PSs across the Tibetan Plateau (Main Surface identified by Li et al., 1995), the Yunnan Plateau (PS1), and the Three Gorges region (E'xi Surface mapped by Li et al., 2001).

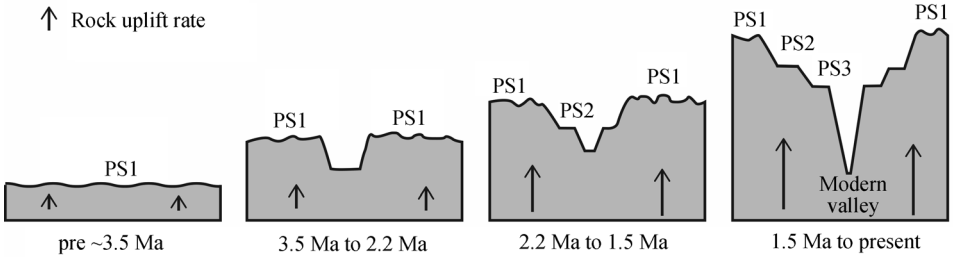

Fig. 13 Idealized profiles illustrating the development of landscape of the UYRB in the SYR.

River began to cut down its own valleys from the PSs. After that, several terraces developed successively in these valleys during the grade period (Su et al., 2013; He et al., 2015).

6 Conclusions

This study identified and quantitatively analyzed the remnants of PSs of the UYRB in the SYR using a DEM-based fuzzy logic method combined with topographic and river profile analysis. Employing a comprehensive analysis of the four morphometric parameters (i.e., slope, curvature, TRI, and RH), we established their fuzzy membership functions and calculated the MD values of this area. We selected the patches with a MD $>$ 80% and an area $>$ 0.4 km^2 as the most likely PSs remnants. Based a detailed analysis of the spatial distribution and morphological elements of these PS remnants, we concluded that they are most probably the remnants of the regionally continuous PSs on which the networks of the Upper Yangtze River cut down its own valleys. Based on the analysis of topographical and longitudinal river profiles, combined with field observations, we found that three levels of PS (labeled PS1 to PS3) had been well developed during three long-time erosion phases. In addition, we calculated the amount of river incision by reconstructing the paleo river profile of each PS. Combining these with erosion rates, the time of formation of PS1, PS2, and PS3 were estimated to be 3.47 Ma, 2.19 Ma, and 1.45 Ma, respectively. In the future, the accurate dating of these PSs will be required for deeper understanding of this region's long-term geomorphological evolution history.

Acknowledgements We should like to thank Dongsheng GUAN for his assistance during fieldwork. We acknowledge Xiaofei HU and Sean F. GALLEN for their help in conducting river profile analyses, Wentao QI for his help in terrain analysis. We thank Paul BESSIN from Le Mans University and other anonymous reviewers for their valuable comments and helpful suggestions. We are grateful to Edward Derbyshire for editing language for the manuscript. This research was supported financially by the National Natural Science Foundation of China (Grant Nos. 41471008 and 41730637) and the United Fund of the National Scientific Foundation of China and Yunnan Province (U0933604), and the Fundamental Research Funds for the Central Universities (lzujbky-2013–272).

References

Adams G F (1975). Planation surfaces: peneplains, pediplains, and etchplains. Benchmark Paper in Geology 22. Stroudsburg PA: Dowden, Hutchington and Ross, 476

Ahnert F (1998). Introduction to Geomorphology. London: Amold

Bascom F (1921). Cycles of erosion in the Piedmont province of Pennsylvania. J Geol, 29(6): 540–559

Bessin P, Guillocheau F, Robin C, Schroëtter J M, Bauer H (2015). Planation surfaces of the Armorican Massif (western France): denudation chronology of a Mesozoic land surface twice exhumed in response to relative crustal movements between Iberia and Eurasia. Geomorphology, 233: 75–91

Bishop P (2007). Long-term landscape evolution: linking tectonics and surface processes. Earth Surf Process Landf, 32(3): 329–365

Bonow J M (2004). Palaeosurfaces and palaeovalleys on North Atlantic previously glaciated passive margins: reference forms for conclusions on uplift and erosion. Institutionen för naturgeografi och kvartärgeologi

Bonow J M, Japsen P, Lidmar-Bergström K, Chalmers J A, Pedersen A K (2006a). Cenozoic uplift of Nuussuaq and Disko, West Greenland—Elevated erosion surfaces as uplift markers of a passive margin. Geomorphology, 80(3–4): 325–337

Bonow J M, Japsen P, Nielsen T F (2014). High-level landscapes along the margin of southern East Greenland—A record of tectonic uplift and incision after breakup in the NE Atlantic. Global Planet Change, 116(2): 10–29

Bonow J M, Lidmar-Bergström K, Japsen P (2006b). Palaeosurfaces in central West Greenland as reference for identification of tectonic movements and estimation of erosion. Global Planet Change, 50(3–4): 161–183

Bosch G V, Van Den Driessche J, Babault J, Robert A, Carballo A, Le Carlier C, Loget N, Prognon C, Wyns R, Baudin T (2016). Peneplanation and lithosphere dynamics in the Pyrenees. C R Geosci, 348: 194–202

Burrough P A, McDonell R A (1998). Principles of geographical information systems. New York: Oxford University Press, 190

Calvet M, Gunnell Y, Farines B (2015). Flat-topped mountain ranges: their global distribution and value for understanding the evolution of mountain topography. Geomorphology, 241: 255–291

Chen F B (1992). Hengduan event: an important tectonic event of the Late Cenozoic in Eastern Asian. Mountain Research, 10(1): 195–202

Clark M K, House M A, Royden L H, Whipple K X, Burchfiel B C, Zhang X, Tang W (2005). Late Cenozoic uplift of southeastern Tibet. Geology, 33(6): 525–528

Clark M K, Royden L H (2000). Topographic ooze: building the eastern margin of Tibet by lower crustal flow. Geology, 28(8): 703–706

Clark M K, Royden L H, Whipple K X, Burchfiel B C, Zhang X, Tang W (2006). Use of a regional, relict landscape to measure vertical deformation of the eastern Tibetan Plateau. J Geophys Res, 111(F3): F03002

Clark M K, Schoenbohm L M, Royden L H, Whipple K X, Burchfiel B C, Zhang X, Tang W, Wang E, Chen L (2004). Surface uplift, tectonics, and erosion of eastern Tibet from large-scale drainage patterns. Tectonics, 23(1): TC1006

Clift P D, Sun Z (2006). The sedimentary and tectonic evolution of the Yinggehai – Song Hong basin and the southern Hainan margin, South China Sea: implications for Tibetan uplift and monsoon intensification. J Geophys Res, 111(B6): B06405

Coltorti M, Firuzabadi D, Borri A, Fantozzi P, Pieruccini P (2015). Planation surfaces and the long-term geomorphological evolution of Ethiopia. In: Billi P, eds. Landscapes and Landforms of Ethiopia. Springer Netherlands, 51(6): 117–136

Cui Z J, Li D W, Feng J L, Liu G N, Li H J (2001a). Covered karst, weathering crust and karst planation surface. Sci China Earth Sci, 31 (6): 510–520

Cui Z J, Li D W, Liu G N, Feng J L, Zhang W (2001b). The properties of the lateritic karst weathering crust and the formation environment of planation surfaces in Tibet, Yunnan, Guizhou, and Hunan province. Sci China Earth Sci, 31: 134–141

Davis W M (1889a). The rivers and valleys of Pennsylvania. National Geographic Society, 1: 183–253

Davis W M (1889b). Topographic development of the Triassic formation of the Connecticut Valley. American Journal of Science, 3rd Ser., 37: 423–434

Davis W M (1899). The geographical cycle. Geogr J, 14(5): 481–504

Feng J L, Cui Z J, Zhang W, Li D W, Liu G N, Zhu L P (2004). Genesis of the layered landform surfaces in Dongchuan, Yunan Province. J Mt Sci, 22(2): 165–174

Flint J J (1974). Stream gradient as a function of order, magnitude, and discharge. Water Resour Res, 10(5): 969–973

Foster M A, Kelsey H M (2012). Knickpoint and knickzone formation and propagation, South Fork Eel River, northern California. Geosphere, 8(2): 403–416

Guillocheau F, Simon B, Baby G, Bessin P, Robin C, Dauteuil O (2018). Planation surfaces as a record of mantle dynamics: the case example of Africa. Gondwana Res, 53(1): 82–98

Hack J T (1973). Stream-profile analysis and stream-gradient index. J Res US Geol Surv, 1(4): 421–429

Haider V L, Dunkl I, Eynatten H V, Ding L, Frei D, Zhang L Y (2013). Cretaceous to Cenozoic evolution of the northern Lhasa Terrane and the Early Paleogene development of peneplains at Nam Co, Tibetan Plateau. J Asian Earth Sci, 70–71(1): 79–98

Haider V L, Kropáček J, Dunkl I, Wagner B, von Eynatten H (2015). Identification of peneplains by multi-parameter assessment of digital elevation models. Earth Surf Process Landf, 40(11): 1477–1492

Harkins N, Kirby E, Heimsath A, Robinson R, Reiser U (2007). Transient fluvial incision in the headwaters of the Yellow River, northeastern Tibet, China. J Geophys Res Earth Surf, 112(F3), https://doi.org/10.1029/2006JF000570

He Z, Zhang X, Bao S, Qian Y S, Sheng Y Y, Liu X T, He X L, Yang X C, Zhao J X, Liu R, Lu C Y (2015). Multiple climatic cycles imprinted on regional uplift-controlled fluvial terraces in the lower Yalong River and Anning River, SE Tibetan Plateau. Geomorphology, 250: 95–112

Hetzel R, Dunkl I, Haider V, Strobl M, Von Eynatten H, Ding L, Frei D (2011). Peneplain formation in southern Tibet predates the India-Asia collision and plateau uplift. Geology, 39(10): 983–986

Huang M H (1992). Research on the stratified landform in the Southwest of China. Journal of Suzhou Railway Teachers College, 9(4): 57–63 (in Chinese)

Huggett R J (2016). Fundamentals of Geomorphology. London: Routledge, 436

Japsen P, Bonow J M, Green P F, Chalmers J A, Lidmar-Bergström K (2009). Formation, uplift and dissection of planation surfaces at passive continental margins—A new approach. Earth Surf Process Landf, 34(5): 683–699

Jarvis A, Reuter H I, Nelson A, Guevara E (2008). Hole-filled SRTM for the globe Version 4. CGIAR-CSI SRTM 90m Database. Available online: http://srtm. csi. cgiar. org

Johansson M (1999). Analysis of digital elevation data for palaeosurfaces in south-western Sweden. Geomorphology, 26(4): 279–295

Jolivet M, Ritz J F, Vassallo R, Larroque C, Braucher R, Todbileg M, Chauvet A, Sue C, Arnaud N, de Vicente RArzhanikova A, Arzhanikov S (2007). Mongolian summits: an uplifted, flat, old but still preserved erosion surface. Geology, 35(10): 871–874

Kennan L, Lamb S, Hoke L (1997). High-altitude palaeosurfaces in the Bolivian Andes: evidence for late Cenozoic surface uplift. Geol Soc Lond Spec Publ, 120(1): 307–323

King L C (1962). Morphology of the Earth. Edinburgh: Oliver and Boyd

Kirby E, Regalla C, Ouimet W B, Bierman P R (2010). Reconstructing temporal variation in fault slip from footwall topography: an example from Saline valley, California, 2010 Fall Meeting, American Geophysical Union, San Francisco, CA

Kirby E, Whipple K X (2012). Expression of active tectonics in erosional landscapes. J Struct Geol, 44: 54–75

Kühni A, Pfiffner O A (2001). The relief of the Swiss Alps and adjacent areas and its relation to lithology and structure: topographic analysis from a 250-m DEM. Geomorphology, 41(4): 285–307

Legrain N, Stüwe K, Wölfler A (2014). Incised relict landscapes in the Eastern Alps. Geomorphology, 221: 124–138

Lei C, Ren J Y, Sternai P, Fox M, Willett S, Xie X N, Clift P D, Liao J H, Wang Z F (2015). Structure and sediment budget of Yinggehai–Song Hong basin, South China Sea: implications for Cenozoic tectonics and river basin reorganization in Southeast Asia. Tectonophysics, 655: 177–190

Li C, Jiang X, Gong W, Li D, Li C (2018). Surface uplift of the Central Yunnan Plateau since the Pliocene. Geol J, 53: 386–396

Li H, Huang X Y, Deng Q L, Kusky T M, Cai X B (2012). Mapping of planation surfaces in the southwest region of Hubei Province, China—Using the DEM-derived painted relief model. J Earth Sci, 23 (5): 719–730

Li J J (1999). In memory of Davisian theory of erosion cycle and peneplain: a centurial study in China. Journal of Lanzhou University

(Natural Sciences), 35(3): 157–163

Li J J, Shi Y F, Li B Y (1995). Uplift of the Qinghai-Xizang (Tibet) Plateau and global change. Lanzhou University Press, 1451–1452

Li J J, Xie S Y, Kuang M S (2001). Geomorphic evolution of the Yangtze Gorges and the time of their formation. Geomorphology, 41(2–3): 125–135

Lidmar-Bergström K, Bonow J M, Japsen P (2013). Stratigraphic landscape analysis and geomorphological paradigms: Scandinavia as an example of Phanerozoic uplift and subsidence. Global Planet Change, 100: 153–171

Liu-Zeng J, Tapponnier P, Gaudemer Y, Ding L (2008). Quantifying landscape differences across the Tibetan plateau: implications for topographic relief evolution. J Geophys Res Earth Surf, 113 (F04018): 1–26

Ma Z H, Li X M, Guo B H, Yu H, Ye X Y, Song C H, Li J J (2016). Extraction and analysis of Maxianshan planation surfaces in northeastern margin of the Tibetan Plateau. Acta Geogr Sin, 71(3): 400–411

Miller S R, Sak P B, Kirby E, Bierman P R (2013). Neogene rejuvenation of central Appalachian topography: evidence for differential rock uplift from stream profiles and erosion rates. Earth Planet Sci Lett, 369–370: 1–12

Monkhouse F J, Wilkinson H R (1952). Population Maps and Diagrams. Maps and Diagrams, Methuen, London

Niemann J D, Gasparini N M, Tucker G E, Bras R L (2001). A quantitative evaluation of Playfair's law and its use in testing long-term stream erosion models. Earth Surf Process Landf, 26(12): 1317–1332

Olaya V (2009). Basic land-surface parameters. In: Hengl T, Reuter H I, eds. Developments in Soil Science, 33: 141–169

Pan B T, Hu Z B, Wang J P, Vandenberghe J, Hu X F, Wen Y H, Li Q, Cao B (2012). The approximate age of the planation surface and the incision of the Yellow River. Palaeogeography, Palaeoclimatology, Palaeoecology, 356: 54–61

Peckham S D, Hengl T, Evans J, Wilson J P, Gould M (2011). Profile, plan and streamline curvature: a simple derivation and applications. In: Proceedings of the International Society for Geomorphometry, Redlands, CA. 27–30

Pike R J (2000). Geomorphometry: diversity in quantitative surface analysis. Prog Phys Geogr, 24(1): 1–20

Qian Y, Xiong L, Li J, Tang G (2016). Landform planation index extracted from DEMs: a case study in Ordos Platform of China. Chin Geogr Sci, 26(3): 314–324

Reuter H I, Nelson A, Jarvis A (2007). An evaluation of void-filling interpolation methods for SRTM data. Int J Geogr Inf Sci, 21(9): 983–1008

Rigon R, Rinaldo A, Rodriguez-Iturbe I (1994). On landscape self-organization. J Geophys Res, 99(11): 911–971

Riley S J, DeGloria S D, Elliot R (1999). A terrain ruggedness index that quantifies topographic heterogeneity. Intermt J Sci, 5(1–4): 23–27

Ringrose P S, Migon P (1997). Analysis of digital elevation data for the Scottish Highlands and recognition of pre-Quaternary elevated surfaces. Geol Soc Lond Spec Publ, 120(1): 25–35

Rowberry M D (2012). A comparison of three terrain parameters that may be used to identify denudation surfaces within a GIS: a case study from Wales, United Kingdom. Comput Geosci, 43: 147–158

Rowberry M D, Brewer P A, Macklin M G (2007). The number, form and origin of sub-horizontal surfaces in north Ceredigion, Wales UK. Norwegian Journal of Geology/Norsk Geologisk Forening, 87(1–2): 207–222

Royden L H, Burchfiel B C, King R W, Wang E, Chen Z, Shen F, Liu Y (1997). Surface deformation and lower crustal flow in Eastern Tibet. Science, 276(5313): 788–790

Schoenbohm L M, Whipple K X, Burchfiel B C, Chen L (2004). Geomorphic constraints on surface uplift, exhumation, and plateau growth in the Red River region, Yunnan Province, China. Geol Soc Am Bull, 116(7): 895–909

Sevon W D, Potter N Jr, Crowl G (1983). Appalachian peneplains: an historical review. Earth Sci Hist, 2(2): 156–164

Shackleton R, Chang C (1988). Cenozoic uplift and deformation of the Tibetan Plateau: the geomorphological evidence. Philosophical Transactions of the Royal Society A, 327(1594): 365–377

Shen J, Wang S M, Wang Y, Qiang X K, Xiao H F, Xiao X Y (2010). Uplift events of the Qinghai–Tibetan Plateau and environmental evolution of the southwest monsoon since 2.7 Ma, recorded in a long lake sediment core from Heqing, China. Quat Int, 218(1–2): 67–73

Strobl M, Hetzel R, Ding L, Zhang L, Hampel A (2010). Preservation of a large-scale bedrock peneplain suggests long-term landscape stability in southern Tibet. Z Geomorphol, 54(4): 453–466

Su H, Ming Q Z, Pan B T, Gao H S, Zhang W X, Dong M, Shi Z T (2013). The analysis and discussions on the chronological frame of Jinshajiang River valley-drainage. J Mt Sci, 31(6): 685–692

Van der Beek P, van Melle J, Guillot S, Pêcher A, Reiners P W, Nicolescu S, Latif M (2009). Eocene Tibetan Plateau remnants preserved in the northwest Himalaya. Nat Geosci, 2(5): 364–368

Twidale C R (1976). On the survival of paleoforms. Am J Sci, 276(1): 77–95

Vandenberghe J (2016). From planation surfaces to river valleys. BSGLg, 67: 93–106

Veselský M, Bandura P, Burian L, Harciníková T, Bella P (2015). Semi-automated recognition of planation surfaces and other flat landforms: a case study from the Aggtelek Karst, Hungary. Open Geosciences, 7 (1): 799–811

Wang E, Burchfiel B C (2000). Late Cenozoic to Holocene deformation in southwestern Sichuan and adjacent Yunnan, China, and its role in formation of the southeastern part of the Tibetan Plateau. Geol Soc Am Bull, 112(3): 413–423

Wang E, Burchfiel B C, Royden L H, Chen L, Chen J, Li W, Chen Z (1998). Late Cenozoic Xianshuihe-Xiaojiang, Red River, and Dali fault systems of southwestern Sichuan and central Yunnan, China. Spec Pap Geol Soc Am, 327: 1–108

Wang X, Lu H, Vandenberghe J, Zheng S, van Balen R (2012). Late Miocene uplift of the NE Tibetan Plateau inferred from basin filling, planation and fluvial terraces in the Huang Shui catchment. Global Planet Change, 88– 89: 10–19

Wang Y, Pan B, Gao H, Liu Y (2005). Planation surface extraction and quantitative analysis based on high-resolution digital elevation models. International Geoscience and Remote Sensing Symposium, 8: 5369–5371

Whipple K X, Dibiase R A, Ouimet W B, Forte A M (2017). Preservation or piracy: diagnosing low-relief, high-elevation surface formation mechanisms. Geology, 45(1): 91–94

Widdowson M (1997). The geomorphological and geological importance of palaeosurfaces. Geol Soc Lond Spec Publ, 120(1): 1–12

Wobus C W, Crosby B T, Whipple K X (2006). Hanging valleys in fluvial systems: controls on occurrence and implications for landscape evolution. J Geophys Res, 111(F2): F02017

Xie M (1990). Neotectonic uplift velocity and type along the Changjiang River during Quaternary. Quaternary Sciences, 4: 308–315 (in Chinese)

Xiong L Y, Tang G A, Zhu A X, Qian Y Q (2017). A peak-cluster assessment method for the identification of upland planation surfaces. Int J Geogr Inf Sci, 31(2): 387–404

Yang R, Willett S D, Goren L (2015). In situ low-relief landscape formation as a result of river network disruption. Nature, 520(7548): 526–529

Zadeh L A (1968). Fuzzy algorithms. Inf Control, 12(2): 94–102

Zárate M, Folguera A (2014). Planation surfaces of Central Western Argentina. In: Rabassa J, Ollier C, eds. Gondwana Landscapes in Southern South America. Springer Netherlands, 365–392

Zevenbergen L W, Thorne C R (1987). Quantitative analysis of land surface topography. Earth Surf Process Landf, 12(1): 47–56

Zhang K, Huang Y K (1995). Researches on the planation surfaces in north Guangdong. Trop Geogr, 15(4): 295–305

Zhang Y C, Li J J, Zhu J J, Kuang M S, Chen Y (1999). Studies on development of Yuanmou basin and valleys during Late Cenozoic. Journal of Lanzhou University (Natural Sciences), 35(1): 199–205

Zheng H, Clift P D, Wang P, Tada R, Jia J, He M, Jourdan F (2013). Pre-Miocene birth of the Yangtze River. Proc Natl Acad Sci USA, 110 (19): 7556–7561

Zhou S, Xu L, Cui J, Zhang X, Zhao J (2005). Geomorphologic evolution and environmental changes in the Shaluli Mountain region during the Quaternary. Chin Sci Bull, 50(1): 52–57

Zhu R X, Potts R, Pan Y X, Lü L Q, Yao H T, Deng C L, Qin H F (2008). Paleomagnetism of the Yuanmou Basin near the southeastern margin of the Tibetan Plateau and its constraints on late Neogene sedimentation and tectonic rotation. Earth Planet Sci Lett, 272(1–2): 97–104